Accepted Manuscript

H2O2-assisted photoelectrocatalytic degradation of Mitoxantrone using CuO nanostructured films: Identification of by-products and toxicity

Ana Paula Pereira da Rosa, Rodrigo Pereira Cavalcante, Débora Antonio da Silva, Lucas de Melo da Silva, Thalita Ferreira da Silva, Fábio Gozzi, Enda McGlynn, Anita Brady-Boyd, Gleison Antônio Casagrande, Heberton Wender, Silvio César de Oliveira, Amilcar Machulek Junior

PII:	S0048-9697(18)34056-7
DOI:	doi:10.1016/j.scitotenv.2018.10.173
Reference:	STOTEN 29076
To appear in:	*Science of the Total Environment*
Received date:	31 July 2018
Revised date:	10 October 2018
Accepted date:	12 October 2018

Please cite this article as: Ana Paula Pereira da Rosa, Rodrigo Pereira Cavalcante, Débora Antonio da Silva, Lucas de Melo da Silva, Thalita Ferreira da Silva, Fábio Gozzi, Enda McGlynn, Anita Brady-Boyd, Gleison Antônio Casagrande, Heberton Wender, Silvio César de Oliveira, Amilcar Machulek Junior , H2O2-assisted photoelectrocatalytic degradation of Mitoxantrone using CuO nanostructured films: Identification of by-products and toxicity. Stoten (2018), doi:10.1016/j.scitotenv.2018.10.173

This is a PDF file of an unedited manuscript that has been accepted for publication. As a service to our customers we are providing this early version of the manuscript. The manuscript will undergo copyediting, typesetting, and review of the resulting proof before it is published in its final form. Please note that during the production process errors may be discovered which could affect the content, and all legal disclaimers that apply to the journal pertain.

ACCEPTED MANUSCRIPT

H_2O_2-assisted photoelectrocatalytic degradation of mitoxantrone using CuO nanostructured films: Identification of by-products and toxicity

Ana Paula Pereira da Rosa[1‡], Rodrigo Pereira Cavalcante[1‡], Débora Antonio da Silva[1], Lucas de Melo da Silva[1], Thalita Ferreira da Silva[1], Fábio Gozzi[1], Enda McGlynn[2*], Anita Brady-Boyd[2], Gleison Antônio Casagrande[1], Heberton Wender[3], Silvio César de Oliveira[1], Amilcar Machulek Junior[1**]

(1) Institute of Chemistry, Federal University of Mato Grosso do Sul, Av. Senador Filinto Muller, 1555, CP 549, CEP 79074-460 - Campo Grande, MS, Brazil

(2) School of Physical Sciences, National Centre for Plasma Science and Technology, Dublin City University, Glasnevin, Dublin 9, Ireland

(3) Institute of Physics, Federal University of Mato Grosso do Sul, Av. Costa e Silva s/n, CEP 79070-900 Campo Grande, MS, Brazil

[‡]Ana P. P. da Rosa and Rodrigo P. Cavalcante have contributed equally to this work.

Paper submitted for publication in *Science of the Total Environment*

[*]Corresponding author: E-mail addresses: enda.mcglynn@dcu.ie (E. McGlynn)

[**]Corresponding author: E-mail addresses: machulekjr@gmail.com (A. Machulek Jr.)

ACCEPTED MANUSCRIPT

Abstract

CuO nanostructured thin films supported on silicon with 6.5 cm^2 area (geometric area greater than the studies reported in the literature) were synthesized by a chemical bath deposition technique. The electrodes were characterized by MEV, XRD, XPS, contact angle, cyclic voltammetry and electrochemical impedance spectroscopy analyses. To evaluate the photoelectrochemical properties of the CuO films, photocurrent–voltage measurements were performed using linear voltammetry. The catalytic activities of CuO nanostructures were evaluated by monitoring photodegradation of Mitoxantrone (MTX) under UV-A light irradiation. The method of photoelectrocatalysis (PEC), applying a voltage of 1.5 V and assisted by adding H_2O_2, was undertaken. To the best of our knowledge, no studies on the degradation of anticancer agents using PEC process have been found in the literature. For comparison purposes, experiments were performed under the same conditions by assisted photocatalysis (PC) with H_2O_2 and direct photolysis. CuO deposits consists of a needle-like morphology. The presence of CuO in the tenorite phase was evidenced by XRD and the XPS spectra showed the presence of copper(II) oxide. The increase in current under illumination shows that CuO exhibits photoactivity. The PEC system showed a 75% level of MTX degradation, while the level achieved using PC was 50%. Under UV-A light alone only 3% removal was obtained after 180 min. Up to 10 by-products were identified by chromatography-mass spectrometry (LC-MS) with m/z values ranging between 521 and 285 and a plausible degradation route has been proposed. It is worth mentioning that 9 by-products identified in this work, were not found in the literature in other studies of degradation or products generated as metabolites. The toxicity tests of MTX before and after PEC treatment with

ACCEPTED MANUSCRIPT

Artemia Salina and *Allium Cepa* showed a decrease in the acute toxicity of the medium as the antineoplastic was degraded.

Keywords: Chemical synthesis; CuO/Si heterojunctions; needle-like CuO nanostructures; photoelectrocatalytic activity; anticancer drug; degradation pathways.

ACCEPTED MANUSCRIPT

ACCEPTED MANUSCRIPT

1. Introduction

The pollution of water bodies by chemical contaminants is one of the greatest problems the world is facing today, increasing with every passing year and causing serious and irreparable damage to the earth and population. Globally, about 1 billion people have no access to drink water supply and around 2.6 billion have no basic sanitation (Ibhadon and Fitzpatrick, 2013). Consequently, urban centers are seeking alternative sources of water supply that may supplement variable rainfall and the demand for population growth, and one of the options considered is the supply of drinking water with recycled water after advanced treatment (Rodriguez et al., 2009).

However, various organic compounds such as pharmaceuticals, personal care products, pesticides, flame-retardants, household chemicals and industrial chemicals pose a huge barrier to these applications, since they are resistance to conventional chemical, biological and photolytic processes (Garcia-Segura and Brillas, 2017). As a result, they have been detected in several aquatic environments at concentrations ranging from nanograms to micrograms per liter (Knopp et al. 2016).

The existence of pharmaceuticals in aquatic environments have been receiving increasing attention in the scientific community as potential micropollutants because they are not naturally biodegradable and show “pseudo persistence”, consequently, being found in surface water, groundwater, urban wastewater and also drinking water (Kanakaraju et al., 2018).

Of particular concern among the pharmaceuticals are residues from anticancer agentes (substances that are used to treat cancer) due to their mutagenic, carcinogenic, and genotoxic potential, even at trace levels.

ACCEPTED MANUSCRIPT

Mitoxantrone or (1,4-dihydroxy-5,8-bis[[2-(2-hydroxyethyl)-amino]-ethyl]-amino]-anthraquinone dihydrochloride; MTX) is a synthetic anthracenedione anti-tumor drug and has been extensively used for the treatment of various malignancies such as advanced breast and prostate cancer, lymphoma and leukaemia (Rossato et al. 2013).

MTX is is eliminated from the body in about 6-11% by urine and 25% in feces and the remainder in the metabolized form (Gómez-Canela et al., 2015). Cytostatic drugs and human metabolites are most often directly discharged into the sewage system, without any specific control after being administered in hospitals (Zhang et al., 2013a). In addition, urban wastewaters receive a substantial contribution of excreted anticancer drugs as the result of outpatient treatment (Isidori et al., 2016).

Conventional treatment is not efficient in removing micropollutants (Cristale et al., 2016), including cytostatic drugs and their metabolites, because these compounds are not readily biodegradable, and they may become persistent in sewage sludge and consequently can be released into surface water from effluents (Isidori et al., 2016). It is therefore extremely important to research and develop technologies that are capable of eliminating these harmful compounds.

Heterogeneous catalysis in conjunction with advanced oxidation processes such as semiconductor photocatalysis has emerged as a promising technique for degrading refractory organics (Eswar et al., 2018). Photocatalysis (PC) requires nanomaterials to be excited and produce reactive species such as holes (h_{VB}^{+}), hydroxyl ($HO^{\bullet}$), superoxide ($O_2^{\bullet-}$) and perhydroxyl ($HO_2^{\bullet}$) radicals that are the main agents responsible for the degradation of organic contaminants (Banerjee et al., 2014; Eswar et al., 2018). However, e^{-}/h^{+} recombinations, which severely limits the achievement of high quantum yields, is the main problem that has to be addressed (Chong et al., 2010).

The application of electrochemical advanced oxidation processes (EAOPs) is

ACCEPTED MANUSCRIPT

an alternative solution for the effective removal of refractory emerging contaminants from water (Martínez-Huitle and Panizza, 2018). The environmental application of EAOPs has been the topic of several books and reviews, among the recent publications on these technologies, highlights one review article described by Sirés et al., 2014 and another presented by Brillas and Martínez-Huitle, 2015. Both reviews point to a broad discussion about the concepts related to these technologies and show advantages of their use for the remediation of pollution problems because the electron is a clean reagent.

The modification of photocatalysis through combination with electrochemistry in the so-called photoelectrocatalysis (PEC) method has been a promising alternative capable of minimizing the difficulties posed by PC, such as recombination of e^-/h^+ pairs and post-treatment removal of catalysts (Sirés et al., 2014; Garcia-Segura and Brillas, 2017).

PEC is based on the application of a bias potential in a semiconductor photoanode simultaneously irradiated with photons of energy equal or greater than its band gap (Garcia-Segura and Brillas, 2017) and results ins significant increases in the degradation rates due to the synergy between electrocatalysis and PC (Eswar et al., 2018).

TiO_2 is the most commonly used semiconductor in photocatalytic reactions (Ramos et al., 2015; Cavalcante et al., 2016). However, the photocatalytic activity of TiO_2 is limited to UV region (wavelength <390 nm, only about 3–5% of the solar energy) due to its wide band gap, around 3.2 eV for anatase TiO_2 and 3.0 eV for rutile TiO_2. Consequently, this increases operating costs and thus limits the practical applications of TiO_2 in this technology (Banerjee et al., 2014).

In this context, cupric oxide, CuO, is an alternative to TiO_2 because it can absorb effectively throughout the visible light region due to its direct band gap in the range

ACCEPTED MANUSCRIPT

1.2–1.5 eV (Sreeju et al., 2017). Other characteristics that render CuO attractive as a photocatalyst include high solar absorbance, high optical absorption, high catalytic activity, low thermal emittance, good electrical properties, chemical stability, low toxicity, as well as being readily available and easy to synthesise by a number of different methods (Zhang et al., 2014).

Although many researchers have reported the application of different nanostructures of CuO in PC, such as, Li et al. (2011), Kim et al. (2015), Sreeju et al. (2017), the focus of these studies were the removal of dyes, which are considered as model molecules.

Limited information is available on the efficiency of this catalyst to explore the degradation of more complex molecules, such as pharmaceuticals. To the best of our knowledge, only two previous works studied the application of CuO for drug degradation by photocatalysis using CuO as semiconductor. Liang et al. (2017) synthesized Pt nanoparticles covered CuO nanosheet-like structures (Pt/CuO composite) and investigated their photocatalytic activities in the degradation of chlortetracycline (one of the components in tetracycline antibiotic) under visible light irradiation. Ahmadi et al. (2017) investigated the removal efficiency of the antibiotic ciprofloxacin using CuO nanoparticles. It is worth mentioning that these studies were performed by photocatalysis.

In contrast, only one study was found in the literature using CuO in the absence of TiO_2 junction for PEC. Eswar et al. (2018) evaluated the performance of network structured CuO for removal of tetracycline antibiotic by PC and PEC. In this study, the authors used fluorine doped tin oxide glass slide, platinum foil and calomel were used as working, conter and reference electrodes, respectively in the presence of CuO nanoparticles. The results showed that PEC exhibited a threefold higher rate of

ACCEPTED MANUSCRIPT

antibiotic degradation compared to PC. In this context, limited information has been found in the literature for the use of CuO as working electrode for application in PEC. Consequently, this study is of great importance to contribute to the lack of studies aiming at the application of CuO electrodes as an alternative for replacing the electrodes based on TiO_2, which are well known in the literature (Fu et al. 2009; Su et al. 2016).

In the present paper, we report the synthesis and detailed characterization of CuO nanostructured films and their application as an efficient photocatalyst for the PEC degradation of the emerging contaminant MTX. In addition, the intermediates formed during the PEC degradation were identified and reaction pathways have been proposed. Finally, acute ecotoxicity of the degradation products was evaluated against larvae of microcrustacean *Artemia salina* and *Allium cepa* (onion). This is the first study exploring the degradation of cytostatics drugs througouth PEC includindg also the investigation of the toxicity of the by-products generated from MTX degradation.

2. Material and Methods

2.1.Materials

Silicon wafers with (100) surface orientation were purchased from Wacker-Chemitronic GMBH. Copper(II) chloride dehydrate (≥ 99,00%) was purchased from Sigma-Aldrich. Ammonia solution (28-30%) were obtained from Merck. MTX (98.01% pure) was purchased from Quiral Química do Brasil. The other reagents and solvents (purchased elsewhere) were used as received.

2.2.Synthesis of CuO films

CuO thin films on Silicon (Si) were synthesized by a chemical bath deposition

ACCEPTED MANUSCRIPT

technique based on the reports of Bayansal et al. (2012) and Sultana et al. (2017). It is worth mentioning that in this study the area of the synthesized electrode was larger than that reported by these references used as a basis.

The process of CuO films preparation showing the heterojunction (CuO/Si) is described in Fig. 1. Firstly, Si wafers were cleaved into pieces of similar sizes of ~ 6.5 cm^2 and washed in ethanol for 5 minutes in an ultrasonic bath. After washing, the substrates were rinsed with deionized water and dried in atmospheric air. Then, 250 mL of a 0.1 mol L^{-1} solution of copper chloride was prepared. The solution was stirred at room temperature (25 ± 1 ºC) for 1 h to ensure complete dissolution of the $CuCl_2$. Subsequently, the pH of the solution was increased to ~ 10 with dropwise addition of ammonia solution under constant stirring. In this step, a blue solution corresponding to $Cu(OH)_2$ was then formed. In the subsequent step, the previously cleaned substrates were immersed vertically into the solution and heating was started until the temperature reached 90 ºC in order to convert $Cu(OH)_2$ into CuO. CuO formation was observed by a change in the coloration of the solution from blue to brownish black and finally to black. The substrates were then kept in the CuO solution at 90 °C for 35 minutes. After that, the oxide-coated substrates were cleaned with deionized water in an ultrassonic bath for 5 minutes in order to remove excess CuO particles from the surface. The electrodes were dried in air at room temperature and finally, the obtained electrodes were characterized in detail using several techniques.

Insert Fig.1

ACCEPTED MANUSCRIPT

2.3.Characterization

The surface morphology of the deposits was imaged via scanning electron microscopy (SEM), using a Carl-Zeiss EVO series SEM Instrument. Average thickness and length of the nanostructures were determined using ImageJ software to count the particles seen in TEM images acquired from different fields in the film (Abramoff et al., 2004).

The crystalline phases present in the CuO films were determined by X-ray diffraction (XRD) analysis, which was carried out on a Rigaku Ultima IV diffractometer with CuKα radiation (λ = 1.541874 Å) across a 2θ angular range of 20–80º with a 0.02º step size and measuring time of 3 s per step. The phase identification was carried out with search-match software utilizing the International Centre for Diffraction Database PDF-2 Release 2003 and COD-Inorg REV189751 2017.01.03.

Material surface chemical composition was determined by X-ray photoelectron spectroscopy (XPS) using a VG Microtech electron spectrometer at base pressure of 1×10^{-9} mbar. The photoelectrons were excited with a conventional Al Kα (hν = 1486.7 eV) X-ray source and analysed by an electron energy analyser operating at 20 eV pass energy, yielding an overall resolution of 1.2 eV. All peak analysis presented in this study was performed using the AAnalyzer curve fitting software program version 1.20. All photoemission peaks were charge referenced to the C 1s peak at a binding energy of 285 eV.

The water contact angle was measured with a CAM-Micro (Tantec Inc.) contact angle meter to verify the hydrophobicity/hydrophilicity of the CuO film using the sessile drop method, employing 5 μL water drops in all cases. The analyses were performed at room temperature and the average value reported was the result from ten

ACCEPTED MANUSCRIPT

drops per sample at different locations. The image analysis was performed using the software GIMP (version 2.6.8).

In order to verify the electrochemical properties of CuO films, cyclic voltammetry (CV) and electrochemical impedance spectroscopy (EIS) analysis were performed in a solution containing 0.05 mol L^{-1} of Na_2SO_4 as the support electrolyte at room temperature (25 ± 1 ºC), using an Autolab potentiostat/galvanostat model PGSTAT 128N equipped with FRA2.X module (Ecochemie, Utrecht, The Netherlands) in a conventional three-electrode mode. The configuration was CuO films or a bare Si wafer (geometric area: 6.5 cm^2) as the working electrode, a Pt network as the counter electrode and commercial Ag/AgCl solution as a reference electrode (filled with 3 mol L^{-1} KCl).

For CV measurements the experimental potential range was -0.5 V to +2.5 V, at a scan rate of 50 mV s^{-1} and an equilibrium time of 120 s. The EIS measurements were performed at an open circuit potential of around 0.19 V (on average) with potential perturbation of 25 mV (rms) and a frequency range of 0.01-10^5 Hz, under dark condition.

2.4.Photoactivity studies

A Potentiostat/Galvanostat model VersaStat II (Princeton Applied Research) controlled via Echem software was used to record the linear scan voltammetry plots for measuring photocurrents in order to analyze the photoactivity of the synthesized films. A Pt network was used as an auxiliary electrode, an Ag/AgCl solution, 3 mol L^{-1} KCl, as a reference electrode and the substrates with the CuO films as the working electrode. The reference electrode was used inside a Luggin capillary. The experimental

ACCEPTED MANUSCRIPT

conditions were: potential range = - 0.5 to + 3.5 V; equilibrium time: 15 s; scanning speed: 5 mV s^{-1}; support electrolyte: 0.05 mol L^{-1} Na_2SO_4 solution (350 mL). The working electrode with 6.5 cm^2 area was illuminated using a 18 W UV-A lamp (Dulux L 18W/78 – Osram) with maximum emission in the 350-400 nm range (see emission spectrum of the UV-A lamp in Fig. S1, Supplementary Material), with a flux of 4.95 x 10^{18} photons s^{-1}, experimentally determined by chemical actinometry (Hatchard and Parker, 1956). The system was kept under constant stirring and the lamp was immersed in the solution inside a glass tube. Voltammograms with and without illumination were recorded.

2.5.Photoelectrocatalytic performance

The PEC activities of the CuO film was evaluated by the removal of MTX under visible light irradiation with the assistance of H_2O_2. The PEC experiments were performed in a photocatalytic reactor with a three-electrode accessory. CuO films, a platinum network and an Ag/AgCl electrode, 3 mol L^{-1} KCl, were used as working, counter and reference electrodes, respectively. 350 mL of solution of 20 mg L^{-1} of MTX in 0.05 mol L^{-1} Na_2SO_4 was degraded by applying a potential of 1.5 V using a potentiostat VersaStat II, for a period of up to 360 min. The photoactive area was irradiated by UV-A lamp (the same lamp used to investigate the photoactivity of CuO films, see details in section 2.4). 35 mL of H_2O_2 (100 mg L^{-1}) in Na_2SO_4 0.05 mol L^{-1} was added to the system using a peristaltic pump at a flow rate of 1 mL min^{-1} (±0.5 s) during the experiment. Direct photolysis and PC, under the same conditions, were measured as well.

The concentration of MTX in each sample was analysed using a Unicam UV–Vis

ACCEPTED MANUSCRIPT

spectrophotometer in the range 450–800 nm with a quartz cell (using measurements at the wavelength of maximum absorbance of MTX, 658 nm). The mineralization was measured by total organic carbon (TOC) analysis using a Shimadzu TOC VCPN instrument.

2.6.Analysis for degradation intermediates

For identification of intermediates by liquid chromatography-mass spectrometry (LC-MS), samples were prepared at a ratio of 50% of sample to 50% methanol (LC-MS grade, Panreac). Analyses were carried out by direct injection (V = 1 μL) into a mass spectrometer (UFLC Shimadzu LC-20AD (Detector IES-Q-QTOF microTOF Q-II high-resolution time-of-flight (TOF) mass spectrometer; Bruker Daltonics), operating in positive electrospray ionization mode (ESI(+)-MS) at a spray voltage of 0.8–1.2 V and capillary voltage of 3500 V, at 200 ºC. Spectra were acquired over the m/z 120-1300 range.

2.7.Acute ecotoxicity tests

2.7.1. Acute ecotoxicity to Artemia salina

For these tests, commercial *Artemia salina* cysts were incubated in a solution of synthetic sea salt (30 g L^{-1}) at pH 8-9, with controlled temperature (20 ± 2 °C), and were aerated for 48 h under constant illumination. The larvae obtained (less than 48 h old) were placed in beakers of 50 mL (10 larvae in each beaker) containing the samples diluted at 100%, 50%, 25%, 12.5%, 6.25%, and 3.12% (v:v), at 20 ± 2 °C, and using 16

ACCEPTED MANUSCRIPT

h light/8 h dark photoperiods in a static system (Da Silva et al. 2018). Forty-eight hours later, dead larvae were counted for each test under a magnifying glass and the mortality of each treatment was calculated, obtaining the median lethal concentrations (LC_{50})—i.e., the concentrations that killed 50% of *Artemia salina* larvae after 48 h of exposure. The tests were performed twice for each dilution and residual levels of H_2O_2 were avoided by adding catalase at 1 mg L^{-1} dropwise before the experiment.

The following measurements were performed: (*i*) untreated 20 mg L^{-1} of MTX solution (called NT); (*ii*) treated by the direct photolysis with H_2O_2 (DP); (*iii*) H_2O_2 assisted PC; (*iv*) H_2O_2 assisted PEC with three-hour experiment duration (PEC3h) and (*v*) H_2O_2 assisted photoelectrocatalysis with six-hour experiment duration (PEC6h).

2.7.2. Acute ecotoxicity to Allium cepa

The *Allium cepa* test was performed as described by Da Silva et al. (2018). Common onions (*Allium cepa*) of the same variety and of similar sizes (30-40 g) were purchased from the local market in Campo Grande. Before the beginning of the test, the yellowish-brown outer layer of the bulbs and their dry bottom plate was removed, so as to expose the apices of the primordial root. Bulbs were afterwards placed on the top of the Falcon 15 mL conical centrifuge tubes (one bulb per each tube) filled with mineral water at 25 ± 1°C and placed in the dark until ~ 2-3 cm –long roots are obtained, and then transferred to test solutions for a period of 48 h.

The tests were performed with the same samples previously described for the assay with *Artemia salina*. In each test, the onion with the lowest root growth was discarded, there being five onions in each test, i.e. five replicas per assay. For each sample, the degree of toxicity against *Allium cepa* was evaluated based on root length

ACCEPTED MANUSCRIPT

(or inhibition of root growth). The three longest roots of each bulb were measured to calculate the average length for each test and results were compared with controls (mineral water rather than sample solution).

3. Results and Discussion

3.1.Characterization results

The morphology of the films was investigated by SEM and the resultant images are shown in Fig. 2. It is found that the CuO deposits consists of a needle-like morphology and the nanoneedles have evenly covered the whole region of the Si substrate (geometric area ~ 6.5 cm^2).

The average thickness value of the middle parts of the needle-like nanostructures were 47 ± 12 nm and the average length was 0.48 ± 0.13 μm, which is smaller than some sizes reported in the literature (Bayansal et al. 2012). The size values obtained in this work are similar to those obtained by Xiang et al. (2010). The needle-like hierarchical structure can greatly increase the contact area between CuO and electrolyte, and hence greatly enhance the reactivity of the electrode, thus increasing the photocatalytic process (Xiang et al. 2010).

Insert Fig.2

Fig. 3 shows the XRD analysis result for a CuO film prepared on a Si substrate. All diffraction lines were broad indicating the formation of small crystallites. The diffraction peaks observed at 2θ values of 35.42º, 38.70º, 48.78º, 58.24º, 61.52º, 65.94º,

ACCEPTED MANUSCRIPT

68.10º, 72.14º and 74.96º can be indexed to the monoclinic structure of CuO tenorite phase [space group Cc (9); a = 4.693 Å, b = 3.428 Å, c = 5.137 Å, β = 99.55°; ICSD 80-1916] which is in good agreement with the reported literature (Vidyasagar et al. 2012; Kim et al. 2015; Kim et al. 2016; Mahmood et al. 2017). It is to note that an additional and intense peak at 54.78º was observed. It is reasonable to attribute this peak to monoclinic structure of the hydrated phase of the copper oxide [a = 7.281 Å, b = 5.184 Å, c = 13.156 Å, β = 93.29°; ICSD 36-0545], since it includes the most intense peak at 54.78º and overlaps with four other peaks observed for CuO (35.42, 38.70, 58.24 and 61.52) (Gupta et al., 1982). Possible peaks from Si substrate were not detected.

Insert Fig. 3

The chemical composition and oxidation state of CuO films was probed by XPS and these data are shown in Fig. 4. In Fig. 4A, the XPS survey spectrum of the CuO film contain peaks corresponding to Cu, O, and adventitious C on the surface.

Fig. 4B shows the high resolution XPS pattern of Cu 2p, wherein the characteristic peaks at 934.1 eV and 953.9 eV corresponds to Cu^{2+} $2p_{3/2}$ and $2p_{1/2}$, respectively, which is consistent with other studies (Liang et al. 2017; Sultana et al. 2017; Eswar et al. 2018). The binding energy difference between Cu $2p_{1/2}$ and Cu $2p_{3/2}$ peaks is 19.8 eV, which is in good agreement with literature data that indicate the presence of the CuO phase (Sultana et al. 2017). Besides, the well-defined satellite peaks at 942.5 eV and 965.6 eV can be assigned to the characteristic shake-up satellite observed in the XPS spectrum of CuO. These strong satellite peaks are only present in CuO films and suggest that there is no presence of copper(I) oxide (Cu_2O) in the films (Liang et al. 2017).

ACCEPTED MANUSCRIPT

The O1s spectrum (Fig.4C) is fitted by three Gaussian peaks. The first and most intense fitted peak (labelled as ‘O(i)’ in the figure) at 529.6 eV is due to the lattice O^{2-} (Cu–O) (Sultana et al. 2017; Eswar et al. 2018). The second fitted peak ‘O(ii)’ at 531.2 eV is considered to be due to oxygen defect sites within the films (Li et al. 2017). The least intense peak ‘O(iii)’ at 532.45 eV may be attributed to surface oxygen species such as adsorbed oxygen O− and/or OH-like species, including hydroxyl species (Cu-OH) (Li et al. 2017). It corroborates the observation of copper oxide hydrate presence in the XRD pattern. No peaks related to the Si substrate were identified in the spectrum, indicating the full coverage of CuO on the substrate surface.

Insert Fig. 4

The main route of degradation of the organic compounds present in the solution involves the interaction between $HO^{\bullet}$ radicals generated on the surface of the catalyst with adsorbed organic molecules (Chong et al., 2010). Therefore, the material must have a good interaction with liquids.

One of the factors favoring the surface-solution interaction is the wettability of the semiconductors used as a catalyst. The greater the liquid tendency to cover the area, the greater the chances that the $HO^{\bullet}$ generation and interaction will be effective. The greater the liquid's ability to spread, the greater the area of contact of the liquid with the surface of the solid, the greater the possibility of a good result in the PC or PEC process. In electrocatalytic processes better electrode/electrolyte wettability can enhance ion diffusion on the surface of electrodes and in the interior of bulk electrodes and improve the electrochemical performance significantly (Li et al. 2018). Water contact angle analysis was used to investigate the surface wettability of CuO films. The average result

ACCEPTED MANUSCRIPT

of water contact angle measurement (Θ) for CuO films was 80.15° ± 1.25. This value is attributed to a material with hydrophilic character (Erbil et al. 2014), indicating that the electrode has the capacity to interact well with liquids, and can wet the surface.

Fig. 5 shows the CV results of the nanostructured CuO films in 0.05 mol L^{-1} of Na_2SO_4 electrolyte at a scan rate 50 mV s^{-1}. It can be seen, the nanostructured CuO films shifted the water-splitting potential related to the Si substrate, this phenomenon could overlap the oxidation peaks of Cu(II)/Cu(III) (ca. 0.8 V vs Ag/AgCl) as previously reported (Marioli and Kuwana 1992; Zhang et al. 2013b).

Insert Fig. 5

Nyquist and Bode plots are analyzed to investigate the interfacial charge transfer process across the CuO/solution interface and the effect of nanostructured film of the electrode in this process. Fig. 6A shows the Nyquist plots and the fitted impedance profiles of the CuO fims and Si wafer used as substrate. The symbols represent the experimental data and the dashed lines represent the fitted results. Both the CuO film and the substrate reveal the existence of two semicircles, which are apparent in the high-frequency regions.

The Nyquist plots of CuO film are found to consists of an imperfect semicircle which indicates the existence of a constant phase element (CPE1) and Warburg element (W) due to inhomogeneity (pores on the surface of the thin films) at the electrode/electrolyte surface and dynamic disorder associated with diffusion (Ray et al. 2017).

The properties of the semicircle can be used to interpret the mobility of electrons in the bulk of material as well as at the interface of the electrode and electrolyte

ACCEPTED MANUSCRIPT

(Mahmood et al. 2017). The data appearing in the high frequency range are classically related to charge transfer resistance (Rct) caused by Faradaic reactions occurring between active materials and the liquid electrolyte (Zhang et al. 2018), which suggest that charge transfer resistance controls the kinetics of the redox reactions occurring at the electrode-electrolyte interface.

Fig. 6A shows that, for the CuO film electrode, Rct is smaller than for the bare substrate without the film. From the fitted data, Rct was 1.0563 MΩ for the CuO film and 3.0056 MΩ for the bare Si without the film. The CuO/Si electrode shows a lower Rct compared to the Si electrode, indicating that electron transfer is easier across the CuO–electrolyte interface.

This decrease in charge transfer resistance might be due to an increase in the number of carrier species accumulated at the electrode-electrolyte interface with the deposition of the film on the substrate. Therefore, EIS results indicated the CuO-Si electrode has good electronic transport properties in comparison to bare Si. The steeper line at low frequencies demonstrates the capacitive nature of the electrode (vertical line for an ideal capacitor) (Liu et al. 2016). Additionally, in the low frequency range of the pure Si electrode, the vertical line is even steeper, which indicates that the Si substrate shows more capacitative behaviour compared to the CuO film.

The plot of /Z/ against the frequency of the electrode materials are provided in Fig. 6B. It shows that at high frequencies the impedance decreases for both electrodes, and the impedance of CuO film is about 1.3 fold higher than that of the bare Si electrode at the low frequency region. Fig. 6C presents the phase angle vs. frequency plot. The phase angle is almost 58° for CuO film. This value is less negative when compared to a perfect capacitor (-90°) confirming a lower resistance to charge mobility in the vicinity of the semiconductor at electrolyte and electrode interface (Mahmood et

ACCEPTED MANUSCRIPT

al. 2017). Also, we can observe a proximity of the vertical line at low frequency region of the Bode plot for bare Si electrode with maximum in 70º, which confirms a better pseudo capacitive nature of the Si material before deposition of the CuO film.

Insert Fig. 6

3.2.PEC performance

Fig. 7 demonstrates the current-potential responses of CuO/Si and bare Si electrodes in the dark and under illumination. As previously described, the photocurrent is associated with the photogenerated electrons moving to the back contact while the photoinduced holes are captured by the hole acceptor in the electrolyte (Mahmood et al. 2017).

The bare Si electrode shows a small photocurrent density (J) of ~ 11.5 µA cm^{-2} at 3.5 V vs. Ag/AgCl. The photocurrent increases significantly with the increase of applied potential. Under UV-A irradiation the resultant current density through the CuO film increases to ~60 µA cm^{-2}, compared to the dark current ~27 µA cm^{-2} at a fixed potential of 3.5 V.

This result can be explained in terms of the CuO film properties. The design of interfacial layers (e.g. insertion of a thin p-CuO layer in Si) is effective in reducing structural disorder, and decreases recombination loss and defect levels (Yoon et al. 2000; Kim et al. 2016). As the valence band of Si is more electropositive compared to that of the CuO film, the hole transfer through the heterojunction (CuO/Si) is more effective, resulting in an increase of the photocurrent (Yoon et al. 2000). Additionally, the better crystallized the film, the less the scattering effects resulting in a better transmission of the incident photons into the structure (Yoon et al. 2000).

ACCEPTED MANUSCRIPT

The increase in current under illumination shows that CuO exhibits photoactivity. Previous works have shown CuO to be a good material to use in PEC cells (Zhang et al. 2014) with values of photocurrent density that depends on the thickness of the CuO films.

The highest photocurrent obtained for the CuO is in agreement with the impedance results. The lower value of Rct for the CuO film compared to Si results in an efficient charge transfer across the electrode-electrolyte interface, there by minimizing charge recombination and enhancing the photocurrent response (Naeem et al. 2015).

In most of the studies in the literature (Mahmood et al. 2017; Oh et al. 2018) CuO films generated cathodic photocurrent under irradiation indicating its p-type conductivity. However, in this study, the *I-V* curves of CuO films unexpectedly generated anodic photocurrent. This behavior is typical feature of *n*-type semiconductor electrodes. Though it is rare, anodic photocurrent generation were reported by other workers (Yoon et al. 2000; Chaudhary et al. 2004; Naeem et al. 2015). Naeem et al. (2015) obtained anodic photocurrent for CuO films and observed that, with increasing applied potential, photocurrent density increases reaching 120 μA cm^{-2} at 0.7 V versus Ag/AgCl. Yoon et al. (2000) investigated the PEC properties of CuO thin films on *n*-type silicon electrodes. The *n*-silicon photoelectrode showed enhanced photocurrent-potential properties by forming a copper oxide/*n*-silicon heterojunction. The *I-V* curves demonstrated an increase of the photocurrent with potential increase, demonstrating behavior characteristic of n-type electrodes. In another study, Chaudhary et al. (2004) evaluated the PEC properties of CuO thin film, prepared by spray pyrolysis on conducting glass. In this study, the authors observed that the CuO films prepared were n-type and explained that this may be possible due to the existence of oxygen vacancies

ACCEPTED MANUSCRIPT

in the structure, which may be due to incomplete oxidation taking place at a relatively low synthesis temperature of 300–400°C.

Insert Fig. 7

3.3. PC and PEC properties of CuO/Si electrodes for the degradation of the antineoplastic agent Mitoxantrone.

The decrease in MTX concentration as a function of UV-A irradiation time intervals under different experimental conditions are shown in Fig. 8A. When only UV-A radiation was used no significant reduction of MTX concentration was obtained, while only a slight degradation (about 15%) of MTX can be observed after 180 min using the PEC with the CuO/Si electrode applying a potential of 1.5 V. As shown in Fig. S2 (Suplementary Material), performing experiments varying the potential (0.6 V and 2.5 V) exhibited lower degradation rates compared to voltage of 1.5 V. Besides that, when SO_4^{2-} electrolyte was used in the experimental conditions, other oxidant species like as persulfate can be formed by electro-oxidation of sulfate at high potentials and/or by its reaction with $HO^{\bullet}$ radical (Sirés et al. 2014; Garcia-Segura et al. 2018).

Previous reports (Li et al. 2011; Wang et al. 2016; Zhang et al. 2017) have shown that the presence of H_2O_2 has a positive effect on the photocatalytic effect of CuO. Since the CuO/Si electrode exhibits weak PEC activity because of the fast recombination of photogenerated electron-hole pairs (Wang et al. 2016), H_2O_2 was added into the reaction solution to enhance the photocatalytic activity of CuO. The addition of H_2O_2 decreases the electron-hole recombination rate and consequently increases hole utilization during the PC process (Zhang et al. 2014; Wang et al. 2016),

ACCEPTED MANUSCRIPT

generating greater amounts of $HO^{\bullet}$ radicals. In addition, H_2O_2 can be quickly reduced and converted to $HO^{\bullet}$ radicals after trapping the photogenerated electrons from the surface of catalysts (Wang et al. 2016). The PEC study in the presence of H_2O_2 was carried out applying the potential of 1.5 V, due to this potential exhibited higher degradation rates compared to other voltages (see Fig. S2 in Suplementary Material) in the PEC experiments performed when CuO/Si is used alone.

The degree of degradation increased sharply when CuO/Si was used in combination with H_2O_2. Fig. 8B shows the time-dependent UV–visible spectra of the MTX aqueous solution during PEC degradation using a CuO/Si electrode as catalyst in the presence of H_2O_2 under visible light illumination. It can be seen that the absorbance peaks at 608 and 658 nm are reduced gradually as the exposure time increases from 0 to 180 min. The colour of the MTX solution changed from dark blue to nearly colourless. After 180 min, about 75% of the MTX was degraded in the presence of CuO/Si and H_2O_2 by the PEC technique (see Fig. 8A), while a H_2O_2 assisted PC reached 50% MET removal in 180 min. From these results, we can observe that the lamp was sufficient for activation of the catalyst. From the emission spectrum (Fig. S1, suplementary material) we can verify that the lamp used is polychromatic and emits radiation between 350 and 400 nm, although it has other spectral lines in the visible region (around 545 and 580 nm). In this way, this study demonstrates that the UV-A lamp can be used in substitution of the solar simulator, which is more expensive.

The results obtained for photoelectrodegradation of MTX prove that PEC, using CuO as photocatalyst, is able to degrade not only simple compounds but also more complex organic molecules like antineoplastic agents.

For comparison it was verified the degradation of MTX by electrocatalysis (EC), where EC refers to the wired configuration without light illumination in the presence of

ACCEPTED MANUSCRIPT

H_2O_2. After 180 min, about 30% of the MTX was removed by the EC system. Hence, it can be stated that H_2O_2 assisted EC is a contributor in the process.

When H_2O_2 alone was used only 9% MTX degradation was observed. The degradation of MTX was almost unaffected by H_2O_2 alone due to lower UV-A induced photolysis of H_2O_2.

As a comparison, the bare Si substrate was also investigated as an electrode to quantitatively understand the PEC activity of the CuO film. This blank experiment showed that the degradation rate is 14% in 180 min, indicating that the photoelectrocatalytic activity of Si can be neglected in comparison with the PEC caused by the CuO catalyst film.

Compared conventional TiO_2 materials, the CuO synthesized has less photocatalytic efficiency. Koltsakidou et al. 2017 evaluated the degradation of antineoplastic drug cytarabine by TiO_2 photocatalysis under simulated solar light radiation, and also evaluated the effect of oxidant addition into the semiconductor suspension, conducting experiments in the presence of H_2O_2 and peroxydisulfate ($S_2O_8^{2-}$). The authors obtained high percentages of mineralization after 360 min of experiments (TOC removal ~80%) by all treatments examined.

Calza et al. 2014 investigated the decomposition of two antineoplastic drugs, methotrexate and doxorubicin by heterogeneous photocatalysis TiO_2 Degussa P25 as the photocatalyst. The process of photocatalysis promoted complete removal of drugs in studies within 30 min of irradiation.

Daghrir et al. 2013a evaluate the potential of PEC process using Ti/TiO_2 for the degradation of carbamazepine, an antiepileptic drug used as sedative. TiO_2 photo-anodes were prepared by means of a pulsed laser deposition (PLD) method. The authors obtained in optimized conditions 73.5% ± 2.8% of carbamazepine removal and 21.2% ±

ACCEPTED MANUSCRIPT

7.7% of mineralization. Through this study it can be observed that for materials based on TiO_2 when supported also a reduction of the photocatalytic efficiency is obtained, however it is worth mentioning that the supported materials avoid the step of removing the catalysts that are tedious in practice. The results obtained from the study by Daghrir et al. 2013a using TiO_2 based electrodes were similar to the results obtained in our study. Therefore, CuO electrodes supported in silicon presented good potential for use as a working electrode in PEC assisted with H_2O_2 for the removal of polluting compounds.

Insert Fig. 8

One of the main chalenges on the photoelectrocatalysis, it is the recyclability of the photocatalysts. Thus, the repeated photodegradation of MTX were carried out using the same electrode in PC and PEC system aided by H_2O_2 in order to measure the stability of CuO films. As shown in Fig. S3 (Supplementary Material), there is no significant decrease of the photoelectrocatalytic activity for CuO/Si after three photodegradation cycles. This same behavior it was observed for the PC system. However, after four repetition cycles it was possible to observe a pronounced loss of photoactivity of the electrodes for both techniques.

Comparing with other common catalysts which are used as dispersed nanoparticles in the reaction media (Sonia et al. 2015; Wang et al. 2016), our CuO film deposited on the Si exhibited slight loss efficiency after four cycles, however it is worth noting that the supported catalysts are more conveniently separated and recycled when compared to nanoparticles systems once no laborious centrifugation process are needed.

3.3.1. Intermediates generated from the degradation of MTX by H_2O_2 assisted PEC

ACCEPTED MANUSCRIPT

For the identification of by-products of MTX degradation (using 20 mg L^{-1} MTX treated by H_2O_2 assisted PEC), sample mixtures after 60 min, 90 min and the final sample after 180 min, were analyzed by LC-MS analysis. The mass of each intermediarie was determined from the peaks corresponding to the protonated molecule ($[M+H]^+$). A total of 10 by-products of MTX degradation at m/z 521, m/z 495, m/z 483, m/z 461, m/z 448, m/z 443, m/z 378, m/z 375, m/z 363 and m/z 285 were identified. The LC-MS spectra of generated intermediates are shown in Fig. S4 (Supplementary Material). Table S1 summarizes the experimental m/z value, the empirical formula obtained by the equipment software used and structures proposed for the intermediates. These proposed structures were based on our knowledge of the degradation of pharmaceuticals and other organic compounds, and based upon study of the published data (Machulek et al. 2009; Daghrir et al. 2013b; Cavalcante et al. 2015; Gómez-Canela et al. 2015; Štenglová-Netíková et al. 2018). These intermediates are largey unreported in the literature, except the compound with m/z 443 which has already been identified as a metabolic (Rossato et al. 2013).

The major part of these primary products were hydroxylated due to $HO^{\bullet}$ radicals attacking the carbon chain of the aromatic part of the molecule. Similarly, the hydroxylated intermediates were also identified by other researchers in PEC processes (Daghrir et al. 2013b; Diao et al. 2013).

A schematic showing the proposed mechanism of MTX degradation by the H_2O_2-assisted PEC process is depicted in Fig. 9. The route is initiated by hydroxylation in the anthraquinone part in the MTX molecule, due to the attack of $HO^{\bullet}$ radicals to yield **1** (*m/z* 461). Subsequently loss of 2-(2-Aminoethylamino)ethanol ($H_2NCH_2CH_2NHCH_2CH_2OH$) on intermediate **1** followed by binding of a $HO^{\bullet}$ radical

ACCEPTED MANUSCRIPT

in the anthraquinone results in the formation of product **2** (*m/z* 375). The product identified as **3** (*m/z* 443) was formed by internal cyclisation of the side-chain amino group to the ring C14 atom from the original molecule (Reszka et al. 1996). Further attack by $HO^{\bullet}$ radicals of the intermediate **1** followed by oxidation of the terminal hydroxyl groups of the side chains yields product **4** (*m/z* 521). The product **5** at m/z 285 corresponded to the loss of two molecules of 2-(ethylamino)ethanol ($C_2H_5NHCH_2CH_2OH$) from the C-N bond breakage on the intermediate **1.** The degradation by-product **6** (*m/z* 449) was proposed to be due to hydroxylation of the intermediate **1** followed by loss of ethanol from the C-N cleavage aliphatic carbon. The product identified as compound **7** (*m/z* 363) was generated by the loss of 2-(ethylamino)ethanol following C-N bond breakage on intermediate **6**. The product **8** (m/z 378) was formed by hydroxylation of the anthraquinone on the intermediate **7**, while intermediate **9** was identified at m/z 495 and corresponds to the loss of ammonia from compound **6**, followed by multiple hydroxylation and subsequent oxidation. Finally, the loss of 2-aminoacetic acid (NH_2CH_2COOH) from intermediate **9** (*m/z* 495) followed by multiple attacks by $HO^{\bullet}$ on aliphatic carbon chains and subsequent oxidation generated degradation by-product **10** (*m/z* 482).

Insert Fig. 9

3.3.2. Acute toxicity

Generally the photocatalytic processes are known to successfully degrade pharmaceuticals, but not necessarily to complete mineralization. In this study, the resulting mineralization of MTX molecules was about 8% after 180 min of experiment by the PEC technique using CuO/Si electrode and H_2O_2. This indicates that the toxicity

ACCEPTED MANUSCRIPT

assessment of intermediates is extremely important to determine the efficiency of treatments because these products may be more toxic than parent compound. However, because of the special toxicity of anticancer drugs, this point may be of even greater importance.

The combination of high sensitivity and low-cost, together with the ease and speed of execution, means the tests using *Allium cepa* and *Artemia salina* are widely used to predict the toxicity of persistent pollutants (Libralato et al. 2016). For these reasons assays using as test microcrustaceans *Artemia salina* and *Allium cepa* (onion) were performed to determine the efficiency of PC and PEC treatments in relation to toxicity of MTX and its intermediates. Larval mortality and root growth (phytotoxicity) were assessed for the tests with *Artemia salina* and *Allium cepa*, respectively.

Table 1 shows the root growth results for the *Allium cepa* assays performed with the MTX solutions before and after the treatments by H_2O_2 assisted PC and PEC in comparison to the control (mineral water).

Tests in an untreated MTX solution revealed root growth inhibition of about 70% in relation to the negative control, whereas about 44% inhibition was observed for solution treated with H_2O_2 assisted PEC after six hours.

As can be seen in Table 1 for the samples treated using H_2O_2 assisted PEC after three hours a small increase in root growth was observed in comparison to the untreated sample. However, the increase in root length was insignificant for the samples treated using H_2O_2 assisted PC and by photolysis direct with H_2O_2. Hence the solutions were considered phytotoxic. Only H_2O_2 assisted PEC treatment for six hours was sufficient to cancel the inhibitory effect, since the root growth value is above half the root growth value of the control, which is about 1.3 cm.

ACCEPTED MANUSCRIPT

Based on the results of biotoxicity assay for *Artemia salina* shown in Table 1, it can be observed that the untreated MTX solution showed a greater mortality of organisms which allowed determination of a LC_{50} value of 17.7 mL mL^{-1}. Using the classification of Persoone et al. (2003) which converts LC_{50} values into toxic units (TUs) with the formula $TU = [1/LC_{50}] \times 100$, a TU value of 5.65 was obtained for untreated MTX solution, which is categorized as class III (acute toxicity). In contrast, for the solutions treated by H_2O_2 assisted PEC after three hours the LC_{50} value found was about 3.54 times greater than for the untreated solution, revealing a significant reduction in toxicity, although toxicity class (III) remained unchanged (see Table 1). For the solutions treated by DP and H_2O_2 assisted PC a small decrease of the acute toxicity was observed, as shown by TU values of 2.91 and 2.88, respectively. For *Artemia salina* no decrease in toxicity was observed for the samples treated by H_2O_2 assisted PEC after six hours.

These toxicity reduction results for H_2O_2 assisted PEC degraded samples corroborate with the higher rates of degradation obtained (see red line in Fig. 8A) and consequently the formation of larger amounts of hydroxylated intermediates which are less toxic than the parent compound (see Table S1 and Fig. 9) in agreement with results reported for the degradation of other drugs (Cavalcante et al. 2016; Da Silva et al. 2018).

Insert Table 1

ACCEPTED MANUSCRIPT

ACCEPTED MANUSCRIPT

4. Conclusions

Needle-like CuO nanostructures on silicon with a geometrical area of ~ 6.5 cm^2 have been successfully synthesized by a chemical bath deposition method using copper chloride as a starting material. It is worth mentioning that the area of the electrode prepared in this study is larger than the area of other electrodes reported in the literature. Detailed characterization confirmed the uniformity in both coverage and morphology of the CuO nanoneedles, which are crystalline and have a monoclinic structure. The surface presented suitable properties for use as a photocatalyst, such as photoactivity, hydrophilic behavior, and a large surface area to volume ratio, due to the high aspect ratio needle-like morphology.

CuO nanostructures assisted by a small amount of H_2O_2 showed efficient PEC activity for MTX degradation, under UV-A illumination. PEC results have shown that the degradation rate increased to 75% compared to PC (at 50%) suggesting that the application of bias through electrocatalysis has dramatically improved the catalytic activity compared to PC. In addition, this is the first study to propose a PEC to degrade anticancer agents that are complex and highly cytotoxic molecules.

PEC treatment yielded 10 by-products, while 9 (at m/z 521, m/z 495, m/z 483, m/z 461, m/z 448, m/z 378, m/z 375, m/z 363 and m/z 285) were not reported in the literature. These intermediates, resulting from cleavage of the MTX molecule, included hydroxylated compounds which decreases the acute toxicity *to Artemia salina* and *Allium Cepa*. A complete reaction pathway for MTX degradation has been proposed, involving hydroxylation of the anthraquinone, internal cyclisation of the side-chain amino group, hydroxylation of aliphatic carbon chains followed by oxidation and shortening or addition of fragments in the lateral chain.

ACCEPTED MANUSCRIPT

The results revealed that CuO nanostructure synthesis by chemical bath deposition provides a convenient, rapid, low-cost and simple method to produce efficient photocatalysts for removal of persistent organic compounds.

Acknowledgments

The authors thank the Brazilian funding agencies Conselho Nacional de Desenvolvimento Científico e Tecnológico (CNPq), Coordenação de Aperfeiçoamento de Pessoal de Nível Superior (Capes, Finance Code 001), Fundação de Apoio ao Desenvolvimento do Ensino, Ciência e Tecnologia do Estado de Mato Grosso do Sul as well as the Irish funding agency Science Foundation Ireland (SFI) under the SFI PI programme (Grant No. 13/IA/1955).

ACCEPTED MANUSCRIPT

ACCEPTED MANUSCRIPT

References

Abramoff, M.D., Magalhaes, P.J., Ram, S.J., 2004. Image processing with ImageJ. Biophotonics Int. 11, 36–42. https://dspace.library.uu.nl/handle/1874/204900.

Ahmadi, S., Banach, A., Mostafapour, F.K., Balarak, D., 2017. Study survey of cupric oxide nanoparticles in removal efficiency of ciprofloxacin antibiotic from aqueous solution: adsorption isotherm study. Desalin. Water. Treat. 89, 297-303. https://doi.org/10.5004/dwt.2017.21362.

Bakhshandeh, F., Azarniya, A., Hosseini, H.R.M., Jafari, S., 2018. Are aluminium titanate-based nanostructures new photocatalytic materials? possibilities and perspectives. J. Photochem. Photobiol. A. Chem. 353, 316–324. https://doi.org/10.1016/j.jphotochem.2017.11.043.

Banerjee, S., Pillai, S.C., Falaras, P., O'Shea, K.E., Byrne, J.A., Dionysiou, D.D., 2014. New insights into the mechanism of visible light photocatalysis. J. Phys. Chem. Lett. 5, 2543–2554. https://pubs.acs.org/doi/abs/10.1021/jz501030x.

Bayansal, F., Çetinkara, H.A., Kahraman, S., Çakmak, H.M., Güder, H.S., 2012. Nano-structured CuO films prepared by simple solution methods: Plate-like, needle-like and network-like architectures. Ceramic. Int. 38, 1859-1866. https://doi.org/10.1016/j.ceramint.2011.10.011.

Brillas, E., Martínez-Huitle, C.A., 2015. Decontamination of wastewaters containing

ACCEPTED MANUSCRIPT

synthetic organic dyes by electrochemical methods . An updated review. Appl. Catal. B. 166–167, 603–643. https://doi.org/10.1016/j.apcatb.2014.11.016.

Calza, P., Medana, C., Sarro, M., Rosato, V., Aigotti, R., Baiocchi, C., Minero, C. (2014) Photocatalytic degradation of selected anticancer drugs and identification of their transformation products in water by liquid chromatography–high resolution mass spectrometry. J. Chromatogr. A, 1362, 135–144. https://doi.org/10.1016/j.chroma.2014.08.035.

Cavalcante, R.P., Dantas, R.F., Wender, H., Bayarri, B., González, O., Giménez, J., Esplugas, S., Machulek, A.Jr., 2015. Photocatalytic treatment of metoprolol with B-doped TiO_2: Effect of water matrix, toxicological evaluation and identification of intermediates. Appl. Catal. B. 176–177, 173–182. https://doi.org/10.1016/j.apcatb.2015.04.007.

Cavalcante, R.P., Dantas, R.F., Bayarri, B., Gonzalez, O., Giménez, J., Esplugas, S., Machulek, A.Jr., 2016. Photocatalytic mechanism of metoprolol oxidation by photocatalysts TiO_2 and TiO_2 doped with 5% B: primary active species and intermediates. Appl. Catal. B. 194, 111–122. https://doi.org/10.1016/j.apcatb.2016.04.054.

Chaudhary, Y.S., Agrawal, A., Shrivastav, R., Satsangi, V.R., Dass, S., 2004. A study on the photoelectrochemical properties of copper oxide thin films. Int. J. Hydrogen. Energy. 29, 131–134. https://doi.org/10.1016/S0360-3199(03)00109-5.

ACCEPTED MANUSCRIPT

Chong, M.N., Jin, B., Chow, C.W.K., Saint, C., 2010. Recent developments in photocatalytic water treatment technology: a review. Water. Res. 44, 2997-3027. https://doi.org/10.1016/j.watres.2010.02.039.

Cristale, J., Ramos, D.D., Dantas, R.F., Machulek, A.Jr., Lacorte, S., Sans, C., Esplugas, S., 2016. Can activated sludge treatments and advanced oxidation processes remove organophosphorus flame retardants? Environ. Res. 144, 11–18. https://doi.org/10.1016/j.envres.2015.10.008.

Da Silva, D.A., Cavalcante, R.P., Cunha, R.F., Machulek, A.Jr., de Oliveira, S.C., 2018. Optimization of nimesulide oxidation via a UV-ABC/H_2O_2treatment process: Degradation products, ecotoxicological effects, and their dependence on the water matrix. Chemosphere. 207, 457-468. https://doi.org/10.1016/j.chemosphere.2018.05.115.

Daghrir, R., Drogui, P., Dimboukou-Mpira A., El Khakani M.A., 2013a Photoelectrocatalytic degradation of carbamazepine using Ti/TiO_2 nanostructured electrodes deposited by means of a pulsed laser deposition process. Chemosphere. 93, 2756–2766. https://doi.org/10.1016/j.chemosphere.2013.09.031.

Daghrir, R., Drogui, P., El Khakani, M.A., 2013b. Photoelectrocatalytic oxidation of chlortetracycline using Ti/TiO_2 photo-anode with simultaneous H_2O_2 production. Electrochim. Acta. 87, 18–31. https://doi.org/10.1016/j.electacta.2012.09.020.

Diao, Z., Li, M., Zeng, F., Song, L., Qiu, R., 2013. Degradation pathway of malachite

ACCEPTED MANUSCRIPT

green in a novel dual-tank photoelectrochemical catalytic reactor. J. Hazard. Mater. 260, 585–592. https://doi.org/10.1016/j.jhazmat.2013.05.037.

Ebadi M., Sulaiman M.Y., Mat-Teridi M.A., Basirun W.J., Golsefidi M.A., Sopian K., Sateei A., Mehrabian, R.Z. Efficient photo-electrochemical performance using CuO-based electrodes in aqua medium. 2016. J. Appl. Electrochem. 46, 645–653. https://link.springer.com/article/10.1007/s10800-016-0948-y.

Erbil, H.Y., 2014. The debate on the dependence of apparent contact angles on drop contact area or three-phase contact line: a review. Surf. Sci. Rep. 69, 325–365. https://doi.org/10.1016/j.surfrep.2014.09.001.

Eswar, N.K., Singh, S.A., Madras, G., 2018. Photoconductive network structured copper oxide for simultaneous photoelectrocatalytic degradation of antibiotic (tetracycline) and bacteria (*E. coli*). Chem. Eng. J. 332, 757–774. https://doi.org/10.1016/j.cej.2017.09.117.

Fu, J.F., Zhao, Y.Q., Xue, X.D., Li W.C., Babatunde, A.O. 2009. Multivariate-parameter optimization of acid blue-7 wastewater treatment by Ti/TiO_2 photoelectrocatalysis via the Box–Behnken design. Desalination 243, 42–51. https://doi.org/10.1016/j.desal.2008.03.038.

Garcia-Segura, S., Brillas E., 2017. Applied photoelectrocatalysis on the degradation of organic pollutants in wastewaters. J. Photochem. Photobiol., C. 31, 1-35. https://doi.org/10.1016/j.jphotochemrev.2017.01.005.

ACCEPTED MANUSCRIPT

Garcia-Segura, S., Ocon, J.D., Chong, M.N., 2018. Electrochemical oxidation remediation of real wastewater effluents – A review. Process. Saf. Environ. Prot. 113, 48-67. https://doi.org/10.1016/j.psep.2017.09.014.

Gómez-Canela, C., Campos, B., Barata, C., Lacorte, S., 2015. Degradation and toxicity of mitoxantrone and chlorambucil in water. Int. J. Environ. Sci. Technol. 12, 633–640. https://link.springer.com/article/10.1007/s13762-013-0454-2.

Gupta, A.S., Srivastava, P.C., Aravindakshan, C., Banerjee, B.K., 1982. X-ray and infrared studies of a copper-urea compound. J. Phys. Chem. Solids. 43, 645-650. https://doi.org/10.1016/0022-3697(82)90055-5.

Hatchard, C.G., Parker, C.A. 1956. A new sensitive chemical actinometer - II. Potassium ferrioxalate as a standard chemical actinometer. Proc. R. Soc. A. 235, 518-536. DOI: 10.1098/rspa.1956.0102.

Ibhadon, A.O., Fitzpatrick, P. (2013) Heterogeneous Photocatalysis: Recent Advances and Applications. Catalysts 3:189-218. https://doi.org/10.3390/catal3010189.

Isidori, M., Lavorgna, M., Russo, C., Kundi, M., Žegura, B., Novak, M., Filipič, M., Mišík, M., Knasmueller, S., de Alda, M.L., Barceló, D., Žonja, B., Česen, M., Ščančar, J., Kosjek, T., Heath, E., 2016. Chemical and toxicological characterisation of anticancer drugs in hospital and municipal wastewaters from Slovenia and Spain. Environ Pollut. 219, 275-287.

ACCEPTED MANUSCRIPT

https://doi.org/10.1016/j.envpol.2016.10.039.

Kanakaraju, D., Glass, B.D., Oelgemöller, M., 2018. Advanced oxidation process-mediated removal of pharmaceuticals from water: a review. J. Environ. Manage. 219, 189-207. https://doi.org/10.1016/j.jenvman.2018.04.103.

Knopp, G., Prasse, C., Ternes, T.A., Cornel, P., 2016. Elimination of micropollutants and transformation products from a wastewater treatment plant effluent through pilot scale ozonation followed by various activated carbon and biological filters. Water. Res. 100, 580–592. https://doi.org/10.1016/j.watres.2016.04.069.

Kim, S.H., Umar, A., Kumar, R., Ibrahim, A.A., Kumar, G., 2015. Facile synthesis and photocatalytic activity of cocoon-shaped CuO nanostructures. Mater. Lett. 156, 138–141. https://doi.org/10.1016/j.matlet.2015.05.014.

Kim, H-S., Kumar, M.D., Patel, M., Kim, J., 2016. High-performing ITO/CuO/n-Si photodetector with ultrafast photoresponse. Sens. Actuators, A 252, 35–41. https://doi.org/10.1016/j.sna.2016.11.014.

Koltsakidou, A., Antonopoulou, M., Evgenidou, E., Konstantinou, I., Lambropoulou, D.A. 2017. Cytarabine degradation by simulated solar assisted photocatalysis using TiO_2. Chem. Eng. J. 316, 823–831. https://doi.org/10.1016/j.cej.2017.01.132.

ACCEPTED MANUSCRIPT

Li, A., He, R., Bian, Z., Song, H., Chen, X., Zhou J., 2018. Enhanced lithium storage performance of hierarchical CuO nanomaterials with surface fractal characteristics. Appl. Surf. Sci. 443, 382-388. https://doi.org/10.1016/j.apsusc.2018.03.019.

Li, J., Sun, F., Gu, K., Wu, T., Zhai, W., Li, W., Huang, S., 2011. Preparation of spindly CuO micro-particles for photodegradation of dye pollutants under a halogen tungsten lamp. Appl. Catal., A. 406, 51–58. https://doi.org/10.1016/j.apcata.2011.08.007.

Li, Z., Tong, K., Shi, R., Shen, Y., Zhang, Y., Yao, Z., Fan, J., Thwaites, M., Shao, G., 2017. Reactive plasma deposition of high quality single phase CuO thin films suitable for metal oxide solar cells. Alloys Compd. 695, 3116-3123. https://doi.org/10.1016/j.jallcom.2016.11.338.

Liang, S., Zhou, Y., Wu, W., Zhang, Y., Cai, Z., Pan, J., 2017. Preparation of porous CuO nanosheet-liked structure (CuO-NS) using C_3N_4 template with enhanced visible-light photoactivity in degradation of chlortetracycline. J. Photochem. Photobiol. A. Chem. 346, 168–176. https://doi.org/10.1016/j.jphotochem.2017.06.005.

Libralato, G., Prato, E., Migliore, L., Cicero, A.M., Manfra, L., 2016. A review of toxicity testing protocols and endpoints with *Artemia* spp. Ecol. Indic. 69, 35–49. https://doi.org/10.1016/j.ecolind.2016.04.017.

ACCEPTED MANUSCRIPT

Liu, D., Fu, C., Zhang, N., Zhou, H., Kuang, Y., 2016. Three-dimensional porous nitrogen doped graphene hydrogel for high energy density supercapacitors. Electrochim. Acta. 213, 291–297. https://doi.org/10.1016/j.electacta.2016.07.131.

Machulek, A.Jr., Gogritchiani, E., Moraes, J.E.F., Quina, F.H., Braun, A.M., Oliveros, E., 2009. Kinetic and mechanistic investigation of the ozonolysis of 2,4-xylidine (2,4-dimethyl-aniline) in acidic aqueous solution. Sep. Purif. Technol. 67, 141–148. https://doi.org/10.1016/j.seppur.2009.03.024.

Mahmood, A., Tezcan, F., Kardaş, G., 2017. Photoelectrochemical characteristics of CuO films with different electrodeposition time. Int. J. Hydrogen. Energy. 42, 23268-23275. https://doi.org/10.1016/j.ijhydene.2017.06.003.

Marioli, J.M., Kuwana, T., 1992. Electrochemical characterization of carbohydrate oxidation at copper electrodes. Electrochim. Acta. 37(7). 1187-1197. https://doi.org/10.1016/0013-4686(92)85055-P.

Martínez-Huitle C.A., Panizza, M., Electrochemical oxidation of organic pollutants for wastewater treatment, 2018. Curr. Opin. Electrochem. https://doi.org/10.1016/j.coelec.2018.07.010.

Naeem, R., Yahya, R., Pandikumar, A., Huang, N.M., Misran, M., Arifin, Z., Mazhar, M., 2015. Photoelectrochemical properties of morphology controlled manganese, iron, nickel and copper oxides nanoball thin films deposited by electric field

ACCEPTED MANUSCRIPT

directed aerosol assisted chemical vapour deposition. Mater. Today. Commun. 4 141–148. https://doi.org/10.1016/j.mtcomm.2015.06.004.

Oh, J., Ryu, H., Lee, W.-J., Bae, J.-S., 2018. Improved photostability of a CuO photoelectrode with Ni-doped seed layer. Ceram. Int. 44, 89–95. https://doi.org/10.1016/j.ceramint.2017.09.129.

Persoone, G., Marsalek, B., Blinova, I., Törökne, A., Zarina, D., Manusadzianas, L., Nalecz-Jawecki, G., Tofan, L., Stepanova, N., Tothova, L., Kolar, B., 2003. A practical and user- friendly toxicity classification system with microbiotests for natural waters and wastewaters. Environ. Toxicol. 18, 395–402. https://doi.org/10.1002/tox.10141.

Ramos, D.D., Bezerra, P.C.S., Quina, F.H., Dantas, R.F., Casagrande, G.A., Oliveira, S.C., Oliveira, M.R.S., Oliveira, L.C.S., Ferreira, V.S., Oliveira, S.L., Machulek, A.Jr., 2015. Synthesis and characterization of TiO_2 and TiO_2/Ag for use in photodegradation of methylviologen, with kinetic study by laser flash photolysis. Environ. Sci. Pollut. Res. Int. 22, 774–783. https://link.springer.com/article/10.1007/s11356-014-2678-1.

Ray, I. Mukhopadhyay, R. Pati, Y. Hattori, U. Prakash, Y. Ishii, S. Kawasaki. 2017. Optimization of photoelectrochemical performance in chemical bath deposited nanostructured CuO. J. Alloys. Compd. 695, 3655-3665. https://doi.org/10.1016/j.jallcom.2016.11.374.

ACCEPTED MANUSCRIPT

Reszka, K.J., Chignell, C.F., 1996. Acid-catalyzed oxidation of the anticancer agent mitoxantrone by nitrite ions. Mol. Pharmacol. 50, 1612-1618. http://molpharm.aspetjournals.org/content/50/6/1612.long.

Rodriguez, C., Buynder, P. V., Lugg, R., Blair, P., Devine, B., Cook, A., Weinstein, P., 2009. Indirect Potable Reuse : A Sustainable Water Supply Alternative. Int. J. Environ. Res. Public. Health. 6, 1174-1209. http://www.mdpi.com/1660-4601/6/3/1174.

Rossato, L.G., Costa, V.M., de Pinho, P.G., Arbo, M.D., de Freitas, V., Vilain, L., Bastos M.L., Palmeira, C., Remião, F., 2013. The metabolic profile of mitoxantrone and its relation with mitoxantrone-induced cardiotoxicity. Arch. Toxicol. 87, 1809–1820. https://link.springer.com/article/10.1007/s00204-013-1040-6.

Sirés, I., Brillas, E., Oturan, M.A., Rodrigo, M.A., Panizza, M., 2014. Electrochemical advanced oxidation processes: Today and tomorrow. A review. Environ. Sci. Pollut. Res. 21, 8336–8367. https://doi.org/10.1007/s11356-014-2783-1.

Sonia, S., Poongodi, S., Kumar P.S., Mangalaraj D., Ponpandian, N., Viswanathan, C. 2015. Hydrothermal synthesis of highly stable CuO nanostructures for efficient photocatalytic degradation of organic dyes. Mater. Sci. Semicond. Process. 30, 585–591. https://doi.org/10.1016/j.mssp.2014.10.012.

ACCEPTED MANUSCRIPT

Sreeju, N., Rufus, A., Philip, D., 2017. Studies on catalytic degradation of organic pollutants and anti-bacterial property using biosynthesized CuO nanostructures. J. Mol. Liq. 242, 690–700. https://doi.org/10.1016/j.molliq.2017.07.077.

Štenglová-Netíková, I.R., Petruželka, L., Šťastný, M., Štengl, V., 2018. Anthracycline antibiotics derivate mitoxantrone—destructive sorption and photocatalytic degradation. PLoS ONE 13(3): e0193116 https://doi.org/10.1371/journal.pone.0193116.

Su, Y-f., Wang, G-B., Ku, D.T.F., Chang, M-l., Shih Y-h., 2016. Photoelectrocatalytic degradation of the antibiotic sulfamethoxazole using TiO2/Ti photoanode. Appl. Catal. B. 186, 184–192. https://doi.org/10.1016/j.apcatb.2016.01.003.

Sultana, J., Paul, S., Karmakar, A., Yi, R., Dalapati, G.K., Chattopadhyay, S., 2017. Chemical bath deposited (CBD) CuO thin films on n-silicon substrate for electronic and optical applications: Impact of growth time. Appl. Surf. Sci. 418, 380–387. https://doi.org/10.1016/j.apsusc.2016.12.139.

Vidyasagar, C.C., Naik, Y.A., Venkatesha, T.G., Viswanatha R., 2012. Solid-State Synthesis and Effect of Temperature on Optical Properties of CuO Nanoparticles. Nano-Micro Lett. 4, 73-77. http://dx.doi.org/10.3786/nml.v4i2.p73-77.

Wang, S.B., Wang, X.Q., Zhang, H.L., Zhang, W.B., 2016. Hollow CuO microspheres with open nanoholes: fabrication and photocatalytic properties. J. Alloys Compd. 685, 22-27. https://doi.org/10.1016/j.jallcom.2016.05.257.

ACCEPTED MANUSCRIPT

Xiang, J.Y., Tu, J.P., Zhang, L., Zhou, Y., Wang, X.L., Shi, S.J., 2010. Simple synthesis of surface-modified hierarchical copper oxide spheres with needle-like morphology as anode for lithium ion batteries. Electrochim. Acta. 55, 1820–1824. https://doi.org/10.1016/j.electacta.2009.10.073.

Yang, F., Zhang, X., Yang, Y., Hao, S., Cui, L., 2018. Characteristics and supercapacitive performance of nanoporous bamboo leaf-like CuO. Chem. Phys. Lett. 691, 366–372. https://doi.org/10.1016/j.cplett.2017.11.047.

Yoon, K.H., Choi, W.J., Kang, D.H., 2000. Photoelectrochemical properties of copper oxide thin films coated on an *n*-Si substrate. Thin. Solid. Films. 372, 250-256. https://doi.org/10.1016/S0040-6090(00)01058-0.

Zhang, J., Chang, V.W.C., Giannis, A., Wang, J.-Y., 2013a. Removal of cytostatic drugs from aquatic environment: a review. Sci Total Environ. 445–446, 281–298. https://doi.org/10.1016/j.scitotenv.2012.12.061.

Zhang, J., Zhu, X., Dong, H., Zhang, X., Wang, W., Chen, Z., 2013b. In situ growth cupric oxide nanoparticles on carbon nanofibers for sensitive nonenzymatic sensing of glucose. Electrochimica Acta. 105, 433–438. http://dx.doi.org/10.1016/j.electacta.2013.04.169.

Zhang, J., Cui, Y., Qin, Q., Zhang, G., Luo, W., Zheng, W. 2018. Nanoporous CuO mesocrystals: low-temperature synthesis and improved structure-performance

ACCEPTED MANUSCRIPT

relationship for energy storage system. Chem. Eng. J. 331, 326–334. https://doi.org/10.1016/j.cej.2017.08.089.

Zhang, Q., Zhang, K., Xu, D., Yang, G., Huang, H., Nie, F., Liu, C., Yang, S., 2014. CuO nanostructures: synthesis, characterization, growth mechanisms, fundamental properties, and applications. Prog. Mater. Sci. 60, 208-237. https://doi.org/10.1016/j.pmatsci.2013.09.003.

Zhang, Y., He, J., Shi, R., Yang, P., 2017. Preparation and photo Fenton-like activities of high crystalline CuO fibers. Appl. Surf. Sci. 422, 1042–1051. https://doi.org/10.1016/j.apsusc.2017.06.034.

ACCEPTED MANUSCRIPT

ACCEPTED MANUSCRIPT

Figure Captions

Fig. 1. Schematic illustration of CuO/Si synthesis.

Fig.2. SEM images of needle-like CuO nanostructures deposited on silicon substrates.

Fig. 3. XRD pattern of CuO thin film and identification of the diffraction peaks.

Fig. 4. XPS spectra of CuO films; (A) XPS survey spectrum of CuO; (B) high resolution XPS spectrum of Cu 2p region; (C) high resolution XPS spectrum of O1s region.

Fig. 5. Cyclic voltammetry (CV) curves of CuO films and bare silicon substrate measured in a 0.05 mol L^{-1} Na_2SO_4 electrolyte at 50 mV s^{-1}.

Fig. 6. Electrochemical impedance spectroscopy results of the CuO film and bare Si substrate electrodes in 0.05 mol L^{-1} Na_2SO_4 electrolyte. (A) Nyquist plots (inset shows equivalent circuits), (B) /Z/ vs frequency and (C) Phase angle vs. frequency.

Fig. 7. Current density vs potential plot obtained on bare Si and CuO/Si electrodes in the dark and under UV-A illumination in 0.05 mol L^{-1} Na_2SO_4 electrolyte at a scan rate of 50 mV s^{-1}.

ACCEPTED MANUSCRIPT

ACCEPTED MANUSCRIPT

Fig. 8. (A) MTX degradation curves under different conditions, (B) Typical time-dependent absorption spectra of MTX solution subjected to H_2O_2-assisted PEC treatment using CuO/Si at 1.5 V under UV–A light irradiation.

Fig. 9. Proposed reaction pathway for the degradation of MTX by H_2O_2-assisted PEC treatment.

ACCEPTED MANUSCRIPT

ACCEPTED MANUSCRIPT

Table 1: Acute toxicity of MTX solutions before and after the treatments against *Allium Cepa* and *Artemia salina*.

	Allium Cepa		***Artemia Salina***			
Solution and treatment	**Root length (cm)***	**Relative Inhibition (%) Compared to Control**	**LC_{50} (% v:v)**	**(95% Confidence limits: lower-higher)**	**TU**	**Toxicity class**
negative control (NC)	2.64 ±0.56	-				
Untreated solution	0.8 ±0.32	70.00	17.70	11.71–23.3	5.65	III
DP	0.96 ±0.11	63.63	34.37	28.37–41.58	2.91	III
PC	1.03 ±0.11	61.00	34.70	29.25–41.15	2.88	III
PEC3h	1.11 ±0.26	57.95	60.96	-	1.64	III
PEC6h	1.48 ±0.25	43.93	54.93	20.98–141.7	1.82	III

*Data expressed as mean ± standard deviation for five replicates.

ACCEPTED MANUSCRIPT

ACCEPTED MANUSCRIPT

Highlights

- Needle-like CuO nanostructures were grown on Si substrates using a CBD method.

- High photoelectrocatalytic performance of CuO film is related to its needle-like nanostructure.

- Enhanced H_2O_2-assisted PEC degradation by CuO film electrodes it was demonstrated.

- The MTX drug exhibits high acute toxicity against *Artemia salina* and *Allium cepa*.

- By-products generated by photoelectrocatalysis are substantially less toxic.

ACCEPTED MANUSCRIPT

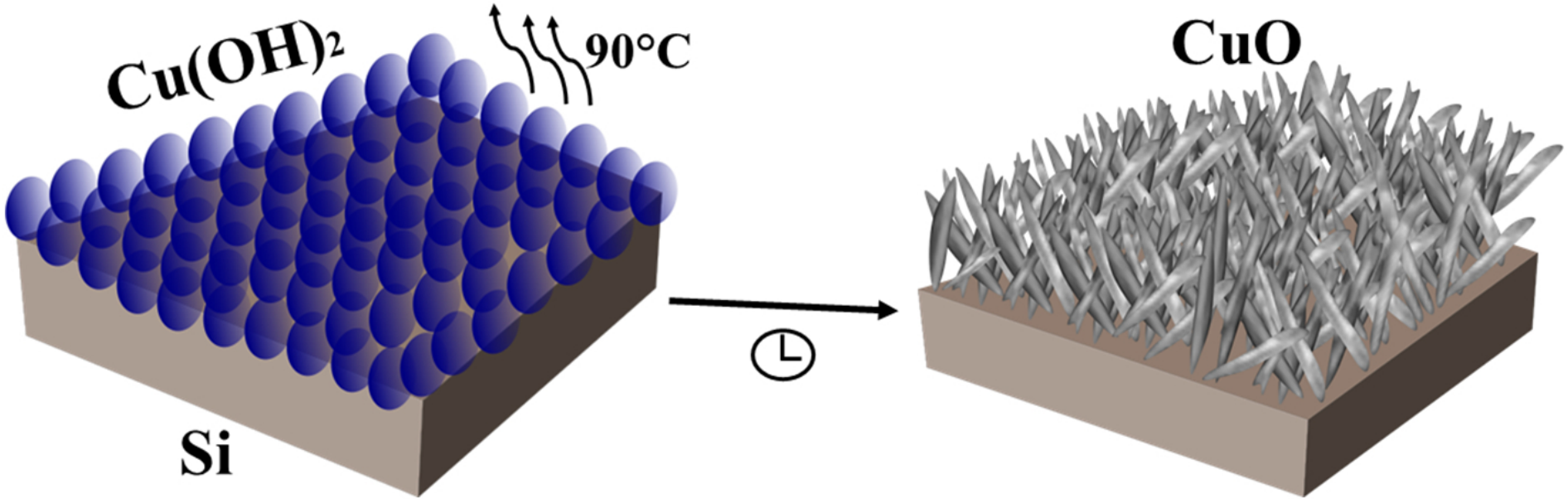

Figure 1

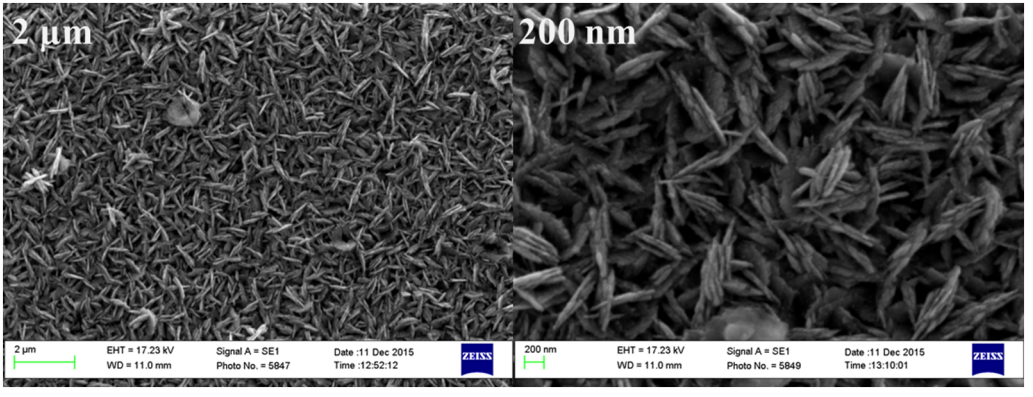
2 µm
2 µm
EHT = 17.23 kV
WD = 11.0 mm
Signal A = SE1
Photo No. = 5847
Date :11 Dec 2015
Time :12:52:12
ZEISS
200 nm
200 nm
EHT = 17.23 kV
WD = 11.0 mm
Signal A = SE1
Photo No. = 5849
Date :11 Dec 2015
Time :13:10:01
ZEISS

Figure 2

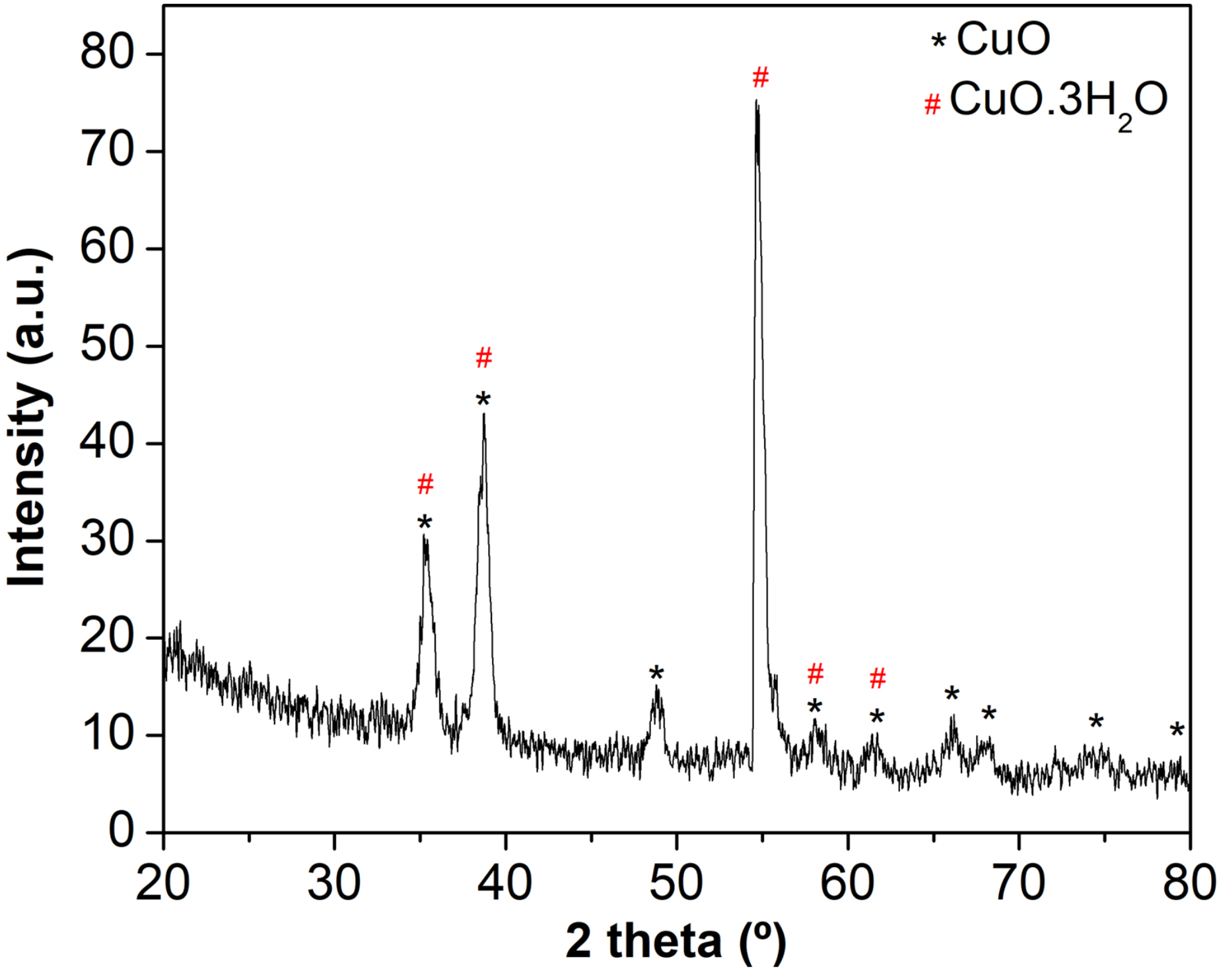
* CuO
# CuO.3H2O
Intensity (a.u.)
2 theta (º)
0
10
20
30
40
50
60
70
80
20
30
40
50
60
70
80

Figure 3

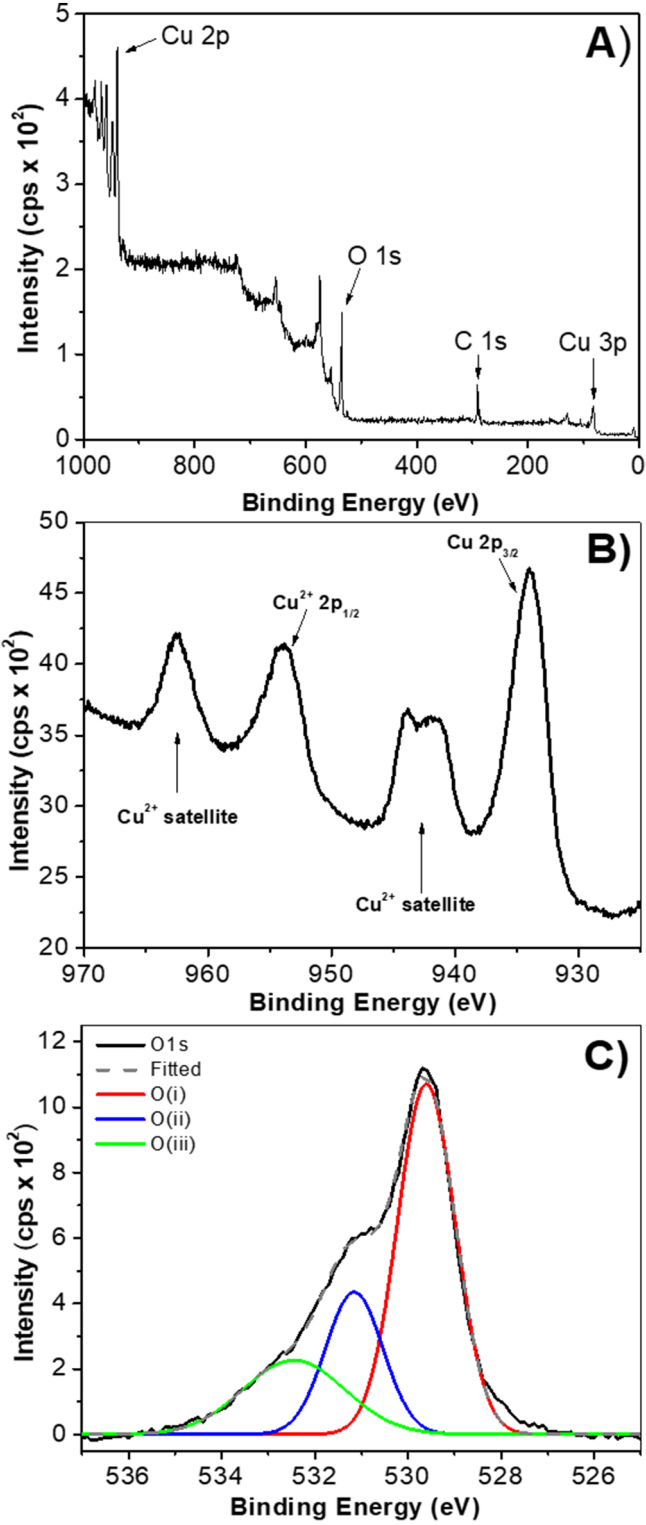
A)
Cu 2p
O 1s
C 1s
Cu 3p
Intensity (cps x 10²)
Binding Energy (eV)
B)
Cu 2p3/2
Cu2+ 2p1/2
Cu2+ satellite
Cu2+ satellite
Intensity (cps x 10²)
Binding Energy (eV)
C)
O1s
Fitted
O(i)
O(ii)
O(iii)
Intensity (cps x 10²)
Binding Energy (eV)

Figure 4

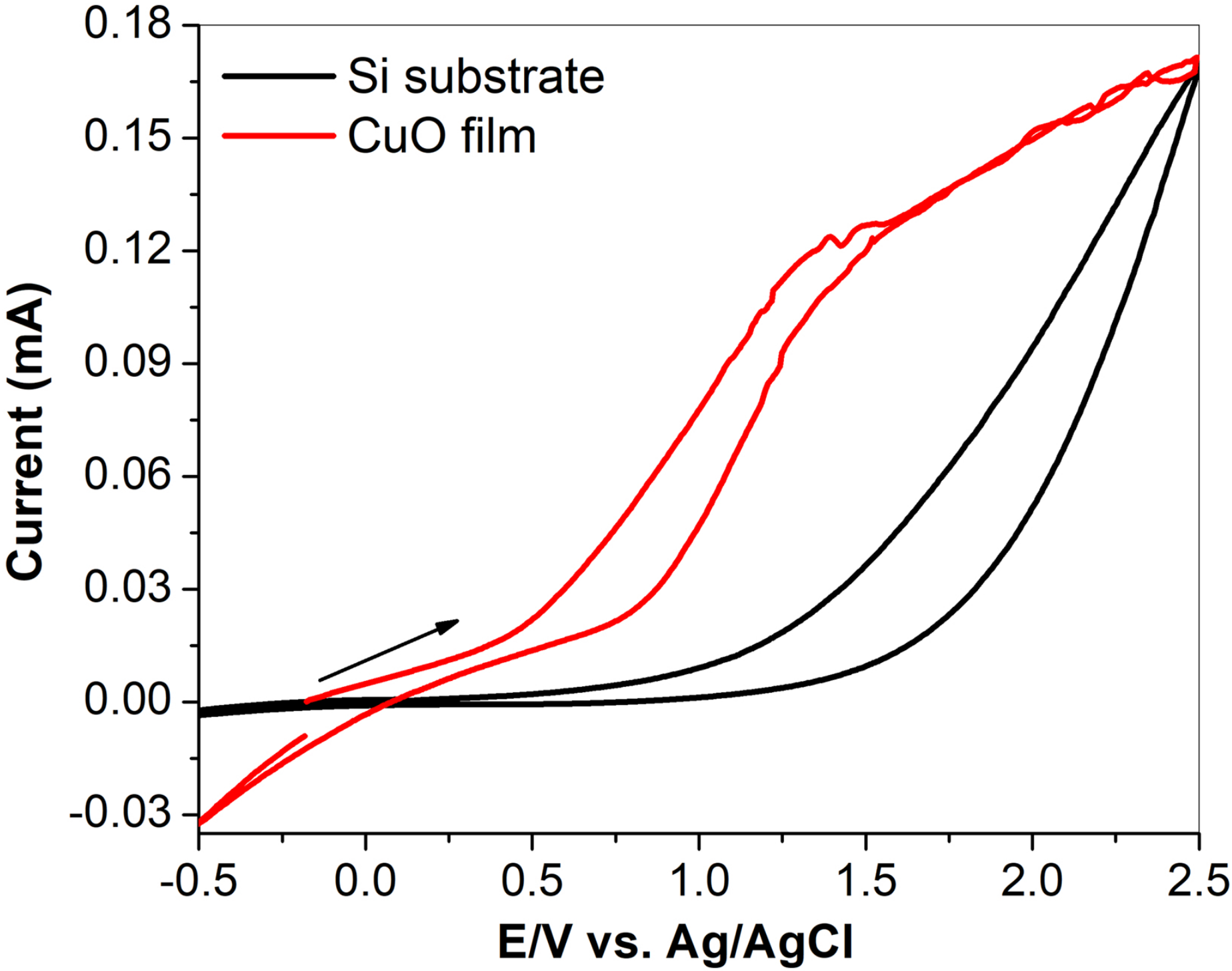
Si substrate
CuO film
Current (mA)
0.18
0.15
0.12
0.09
0.06
0.03
0.00
-0.03
-0.5
0.0
0.5
1.0
1.5
2.0
2.5
E/V vs. Ag/AgCl

Figure 5

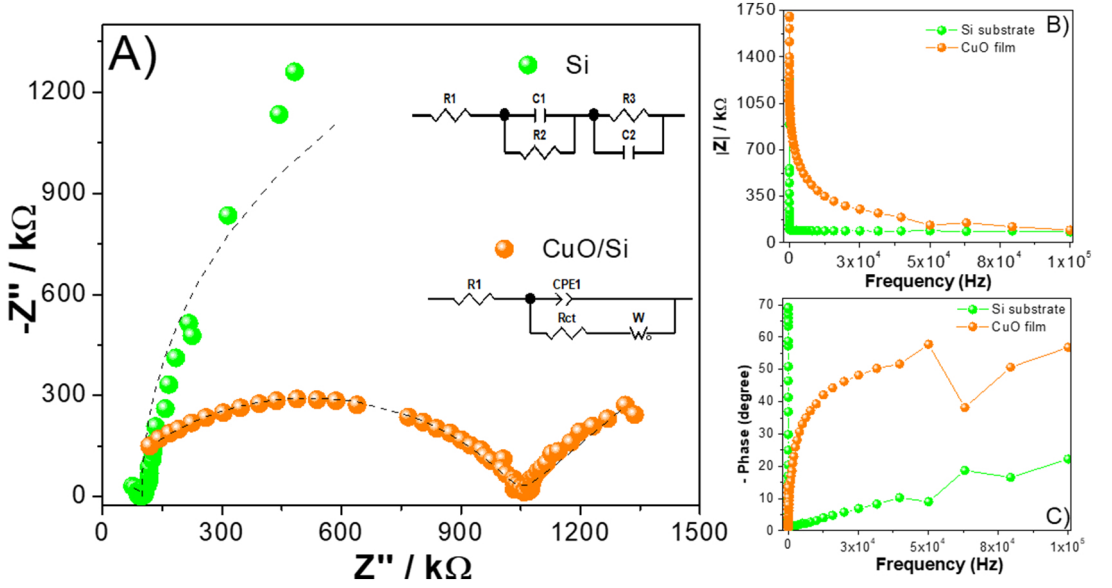
A)
Si
R1
C1
R3
R2
C2
CuO/Si
R1
CPE1
Rct
W
-Z'' / kΩ
Z'' / kΩ
0
300
600
900
1200
1500
B)
Si substrate
CuO film
|Z| / kΩ
Frequency (Hz)
C)
- Phase (degree)
Frequency (Hz)

Figure 6

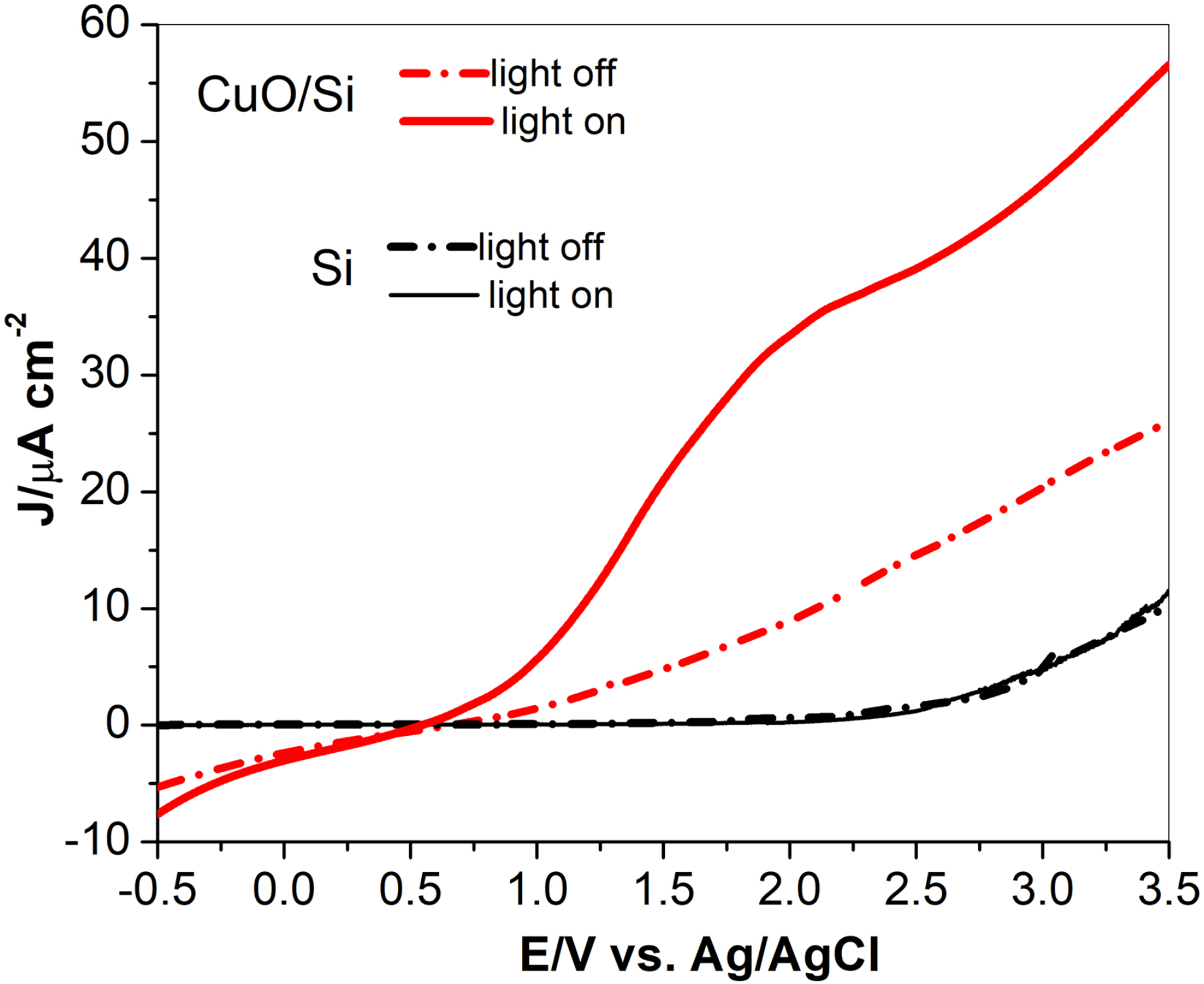
CuO/Si
light off
light on
Si
light off
light on
J/μA cm-2
E/V vs. Ag/AgCl
60
50
40
30
20
10
0
-10
-0.5
0.0
0.5
1.0
1.5
2.0
2.5
3.0
3.5

Figure 7

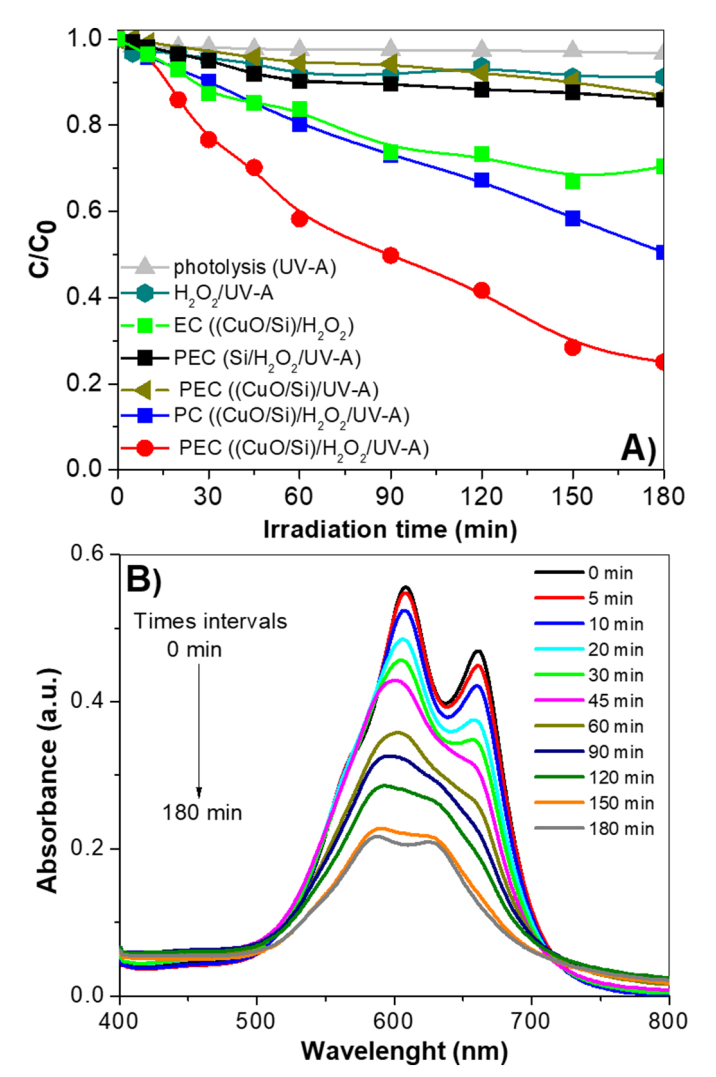
A)
C/C0
Irradiation time (min)
photolysis (UV-A)
H2O2/UV-A
EC ((CuO/Si)/H2O2)
PEC (Si/H2O2/UV-A)
PEC ((CuO/Si)/UV-A)
PC ((CuO/Si)/H2O2/UV-A)
PEC ((CuO/Si)/H2O2/UV-A)
B)
Times intervals
0 min
180 min
Absorbance (a.u.)
Wavelenght (nm)
0 min
5 min
10 min
20 min
30 min
45 min
60 min
90 min
120 min
150 min
180 min

Figure 8

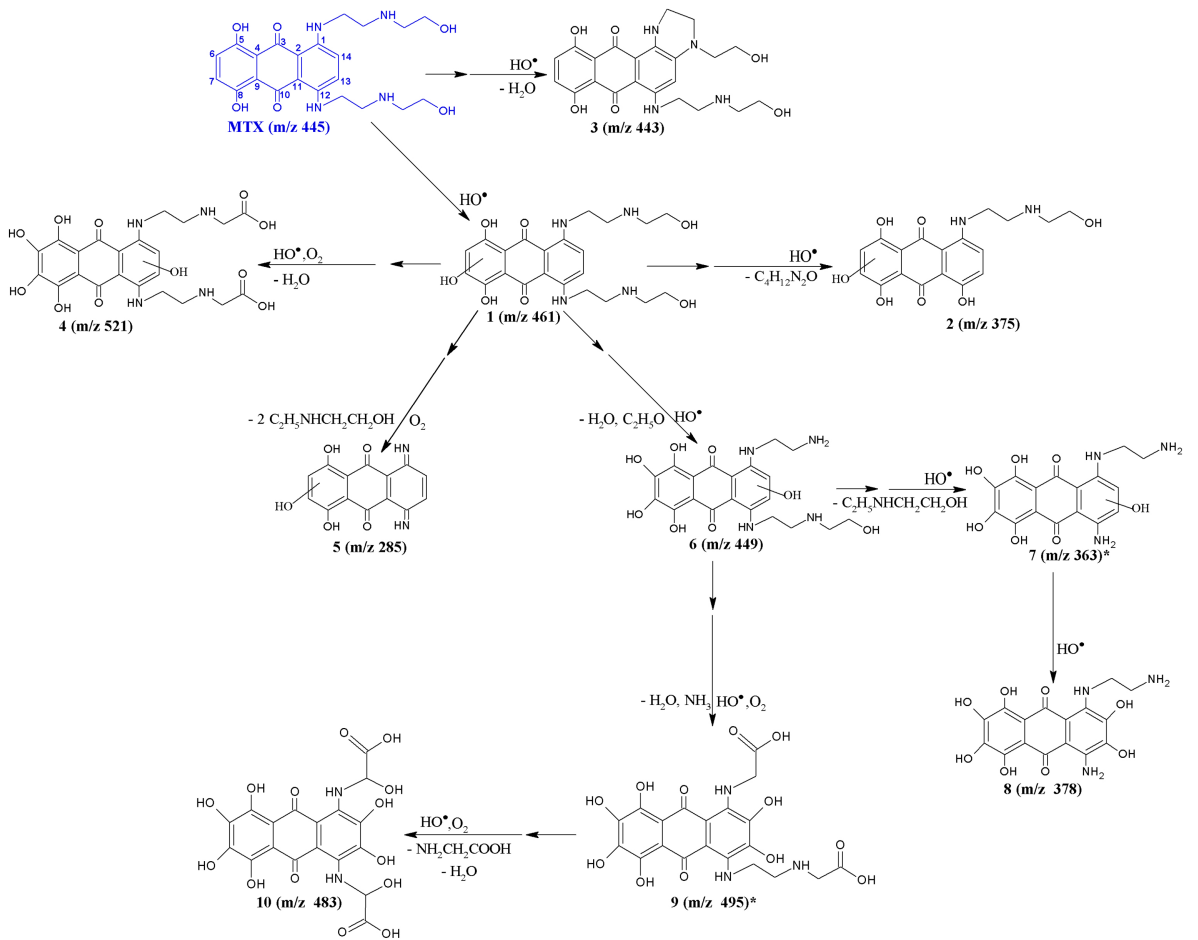

*Compounds with m/z 365 and 495 are diprotonated.

Figure 9